Chapter 5

Study of Two-Stage Coronal Jet Associated with a C1.4 Class Solar Flare

We study an active region coronal jet that evolved from southward of a major sunspot of NOAA AR12178 on 04 October 2014. This jet is associated with an onset of the GOES C1.4 flare. We use SDO/AIA, SDO/HMI, GONG Hα and GOES data for analysing the observed event. We term this jet as a two-stage confined eruption of the plasma. In the first stage, some plasma erupts above the compact flaring region. In the second stage, this eruptive jet plasma and associated magnetic field lines interact with another set of distinct magnetic field lines present in its south-east direction. This creates an X-point region, where the second stage of the jet eruption is deflected above it on a curvilinear path into overlying corona. The lower part of the jet is followed by a cool surge eruption, which is visible only in Hα emissions. The magnetic flux cancellation at the footpoint causes the triggering of C-class flare eruption. This flare energy release further triggers first stage of the coronal jet eruption. The second stage of the jet eruption is a consequence of an interaction of two distinct sets of magnetic field lines in the overlying corona. The first stage of the coronal jet and co-spatial but

lagging cool surge may have common origin due to the reconnection generated heating pulses. This complex evolution of the coronal jet involves flare heating induced first stage plasma eruption, guiding of jet's material above a junction of two distinct sets of field lines in the corona, and intra-relationship with cool surge. In effect, it imposes rigid constraints on the existing jet models.

5.1 Introduction

Solar coronal jets are characterized as the hot and cold plasma ejections from the lower solar atmosphere to its upper layers along the open magnetic field lines (e.g., Chandra *et al.*, 2017; Filippov *et al.*, 2015; Kayshap, Srivastava and Murawski, 2013; Kayshap *et al.*, 2013; Shibata *et al.*, 1992, 2007; Shimojo *et al.*, 2007). These dynamic jets show many properties associated with confined solar transients, which are seen in coronal holes, quiet Sun and active regions (e.g., Nisticò *et al.*, 2009; Panesar *et al.*, 2016; Shimojo *et al.*, 1996). These magnetically driven and confined plasma ejecta have lesser energy compared to "nominal" solar flares and coronal mass ejections (CMEs) (Raouafi *et al.*, 2016). They possess the kinetic energy of about 10^{25}-10^{28} ergs (Shibata *et al.*, 1992). Statistical study of coronal jets as observed in X-rays shows that their typical length and width respectively are 10^4-10^5 km and 10^3-10^5 km. Their speed ranges from 10 to 1000 $\mathrm{km\,s^{-1}}$ with an average velocity of 200 $\mathrm{km\,s^{-1}}$. These jets have life time from a few tens of minutes to hours (Shibata *et al.*, 1992; Shimojo *et al.*, 1996).

With the help of multi-wavelength observations of jets, we can classify them in two categories namely, hot jets (X-ray or EUV jets) and cool jets ($H\alpha$ surge or dark EUV jets). These two categories of jets are almost co-spatial and co-temporal, and are connected with each other dynamically (Nishizuka *et al.*, 2008). The cool solar surges are straight or arch-shaped collimated ejections of plasma material which are usually visible in $H\alpha$ (656

nm) and other chromospheric and coronal lines (Sterling, 2000). Solar surges are cool jets which usually occur in strong magnetic fields existing in and around active regions. The small flares like brightenings are usually found at the base of most of solar surges. The ejected surge material may be linked to the Ellarman bomb brightening near the boundary of strong magnetic field concentration (Roy, 1973; Uddin *et al.*, 2012). In some recent works of Reid *et al.* (2015, 2016) a connection is found between the chromospheric jets and the Ellarman bomb brightening, because there is enough magnetic energy at the Ellarman bomb brightening site which can drive the jet in the upward direction from the photosphere.

The photospheric magnetic field activity and magnetic reconnection are found to be the driving mechanisms for solar surges and other types of cool jets. There are alternative triggering mechanisms for the cool jets and surges, for example, photospheric magnetic field emergence and cancellation (e.g., Gaizauskas, 1996; Sterling, 2000; Uddin *et al.*, 2012), impulsive generation of pressure pulse (Kayshap, Srivastava and Murawski, 2013; Kayshap *et al.*, 2013; Shibata *et al.*, 1982; Steinolfson, Schmahl and Wu, 1979), etc.

There exist many observations which suggest that the magnetic reconnection is most favourable mechanism for the generation of typical solar coronal jets (Shibata *et al.*, 1992, 2007). The numerical simulations of Yokoyama and Shibata (1995, 1996) show that the magnetic reconnection can generate hot and cool jets simultaneously in which fast mode MHD shock is produced. The simulation results of Nishizuka *et al.* (2008) show the generation of Alfvén waves with the formation of jet. The numerical simulation results drawn by Pariat, Antiochos and DeVore (2009) show the signature of kink instability at the jet formation site which may boost the upward motion of jet in the model solar atmosphere. Sometimes it is observed that the fast moving chromospheric jets (spicules) are driven by magneto-acoustic shock waves (Rao *et al.*, 2017; Skogsrud *et al.*, 2015). Hence, the magnetic reconnection and the generated waves can be the most favourable drivers for these kinds of jets.

In the present study, we describe the observational results of a two-stage complex coronal jet eruption associated with C1.4 flare, which is followed by a cool surge eruption as observed on 04 October 2014 in the southward direction of a major sunspot of an active region NOAA AR12178. In Section 5.2, we describe the observational data and its analyses. In Section 5.3, we discuss the observational results, kinematics and possible driving mechanism of two-stage coronal jet and associated cool surge. We also analyse the magnetic field properties at the base of the jet and potential field source surface (PFSS) extrapolation in and around jet activity region. In Section 5.4, we describe possible theoretical interpretation of the evolution of jet and surge. In the last section, we outline discussion and conclusions.

5.2 Observational Data and Its Analyses

We use data from several space-based instruments: Solar Dynamics Observatory (SDO; Pesnell, Thompson and Chamberlin, 2012)/Atmospheric Imaging Assembly (AIA; Lemen *et al.*, 2012) and SDO/Helioseismic Magnetic Imager (HMI; Scherrer *et al.*, 2012). For analysing our event, we download SDO/AIA and SDO/HMI data from Joint Science Operation Center (JSOC) (jsoc.stanford.edu). We use SDO/AIA data for multi-wavelength analysis of two-stage confined coronal jet eruption. AIA instrument which is onboard on SDO observes the Sun in ultraviolet (UV), extreme ultra-violet (EUV), and continuum wavelengths. SDO/AIA observes the full-disk Sun, and it has pixel width of $0.6''$. It operates with 12 sec cadence in EUV channels and 24 sec in UV channels. We use SDO/AIA temporal image data in seven EUV wavelengths: 304 Å , 171 Å , 193 Å , 211 Å , 335 Å , 94 Å and 131 Å and in one UV wavelength: 1600 Å . SDO/AIA data have been taken for 1-h time period from 10:00 UT to 11:00 UT for the particular region of $200'' \times 300''$ in the southward direction of NOAA AR12178 on 04 October 2014. The selected field of view (FOV) of SDO/AIA temporal image data ranging from $100''$ to $300''$

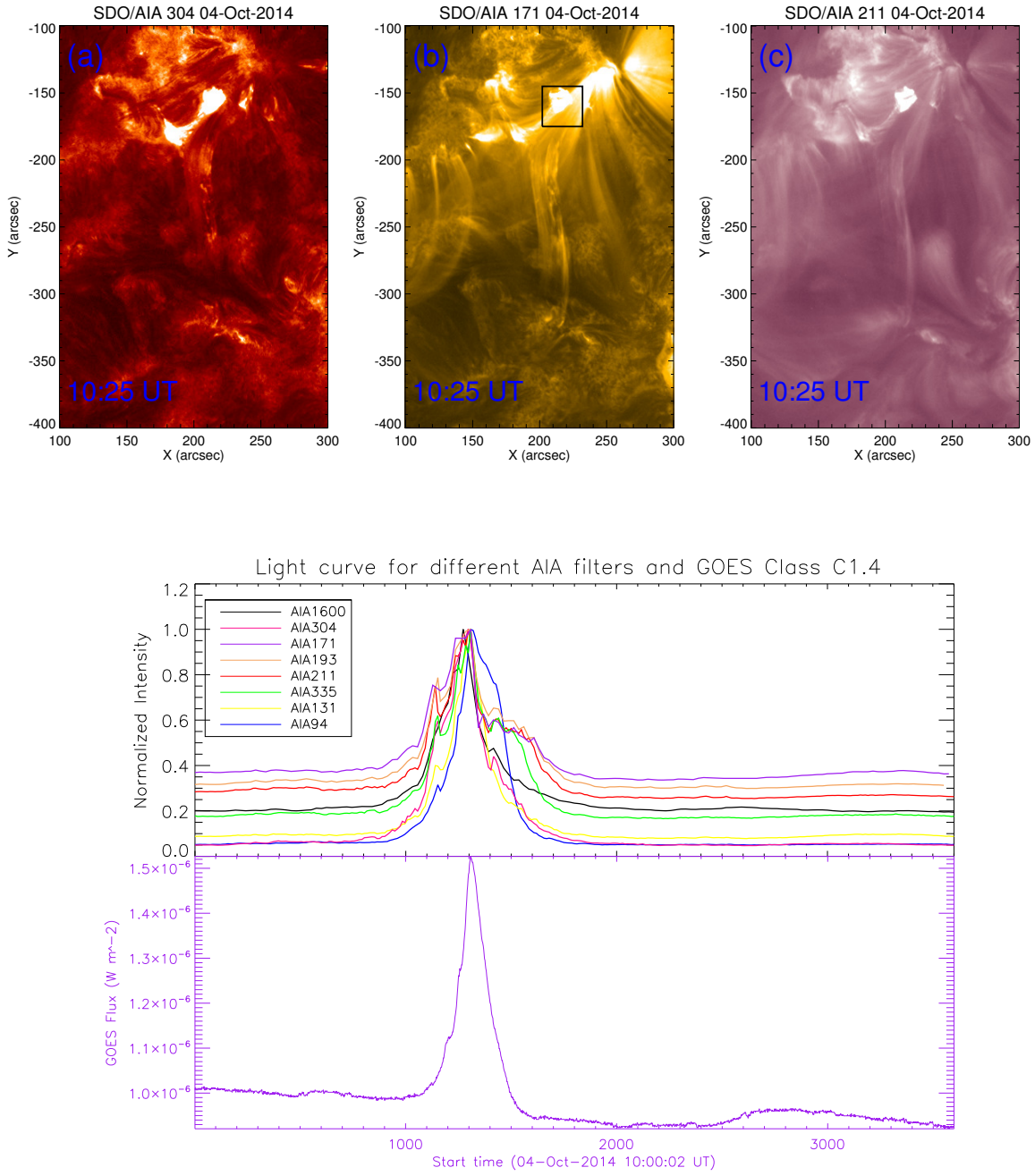

Figure 5.1: In the upper Panel, SDO/AIA images in 304 Å, 171 Å and 211 Å depict the evolution of a confined two-stage coronal jet. Bottom Panel shows the light curves for different AIA filters and GOES X-ray flux class C1.4. These fluxes are derived from the box which is at the footpoint of the evolved jet. The box of the size $30'' \times 30''$ is overplotted on AIA 171 Å image.

in X-direction, and $-400''$ to $-100''$ in Y-direction (see Figure 5.1). The observed events are two-stage confined jet eruption, C1.4 flare, and a cool surge, which have been analyzed in this FOV using multi-wavelength data.

For investigating the possible origin of this complex jet, we also use HMI data, which is another instrument on board SDO. HMI provides line-of-sight maps of photospheric magnetic field with cadence of 45 sec and with pixel width of $0.5''$. We have studied SDO/HMI line of sight (LOS) magnetograms for 1-h time period from 09:59:56 UT to 10:59:56 UT for analysing the topology of underlying magnetic field. SDO/HMI data is analyzed for the same field of view (FOV) as we have choose in SDO/AIA. For scaling and aligning the SDO/AIA images as observed in different filters, we use hmi_prep subroutine of SSW IDL. SDO/HMI data is rotated and aligned with the SDO/AIA data for the same plate scale, as these two instruments have different resolutions.

We use Gong Oscillation Network Group (GONG; Harvey *et al.*, 2011) $H\alpha$ observations for investigating the dynamic evolution of the cool surge. We download GONG $H\alpha$ data from NSO:Global Oscillation Network Group (https://gong.nso.edu) for 1-h time duration from 10:00 UT to 11:00 UT for the particular region of $200'' \times 300''$. The GONG gives full disk images of the Sun in 6563 Å , with spatial resolution of $2''$ and 1 minute cadence. The selected field of view (FOV) of GONG data range from $100''$ to $300''$ in X-direction, and $-400''$ to $-100''$ in Y-direction.

We also use Geostationary Operational Environmental Satellites (GOES; Garcia, 1994) data for studying emitted soft X-ray flux in C1.4 flare. GOES are a series of satellites which are maintained by the National Oceanic and Atmospheric Administration (NOAA). These satellites contain two X-ray sensors (XRS) which monitor the solar flux in two wavelength bands 1 Å - 8 Å and 0.5 Å - 4 Å .

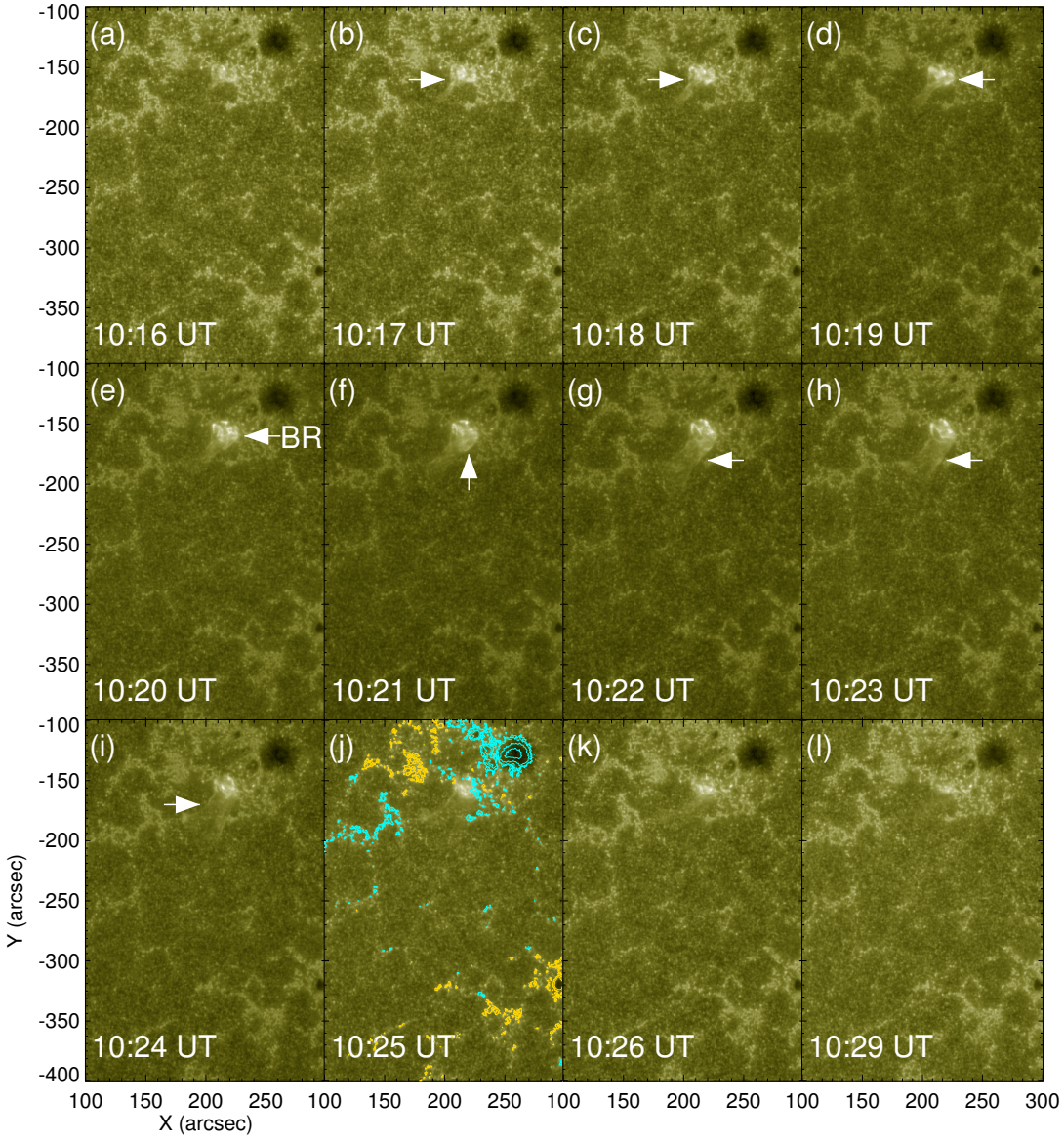

Figure 5.2: Sequence of selected SDO/AIA 1600 Å images showing a C1.4 flare evolution. This location also triggers the first stage of a complex coronal jet (cf., Figures 5.3 - 5.4). Photospheric magnetic field contours are overlaid on SDO/AIA 1600 Å image at 10:25 UT. Cyan color shows positive polarity and gold color shows the negative polarity with contour levels ±100, ±200, ±300, ±750, ±1400 G.

5.3 Observational Results

5.3.1 Analysis of Time-intensity Profile at the Footpoint of Evolved Jet

In Figure 5.1, the upper panel shows a jet eruption in different SDO/AIA wavelengths at 10:25 UT. These SDO/AIA images in AIA 304 Å , AIA 171 Å , AIA 211 Å collectively signify the presence of multi-temperature plasma in the jet. The selected field of view (FOV) for these images is $100''$ to $300''$ in X-direction, and $-400''$ to $-100''$ in Y-direction.

Upper part of the bottom panel in Figure 5.1 shows an intensity lightcurve from different AIA channels during the observational period of the jet between 10:00 UT to 11:00 UT. We have plotted the normalized intensity (mean intensity/max intensity) and observational period, where starting time is 10:00 UT. The intensity is extracted at the footpoint of the jet from the black box, which is overplotted on SDO/AIA 171 Å image as shown in upper panel of Figure 5.1. Box size is taken as $30''\times 30''$. Normalized intensities for different AIA filters vary in the time period of 10:15 UT to 10:30 UT, and besides this period intensities are almost constant for all filters (which is equilibrium state of this region with surrounding). Variation in intensity in different filters shows nearly same behaviour. We have noted that there are multiple peaks at 10:19 UT, 10:21 and 10:24 UT in intensity curve, and intensities reach its highest value for this region at 10:21 UT in all filters of AIA. In the lower part of the bottom panel of Figure 5.1, GOES C1.4 light curve in soft X-ray range 1 Å - 8 Å , is displayed for the same time duration as in SDO/AIA light curve. GOES flare starts at 10:16 UT and peaks at 10:21 UT, and disappears at 10:24 UT. So the total time duration of this flare is 8 min and the emitted X-ray flux is of the order of $10^{-6}Wm^{-2}$, which is the C1.4 class flare flux order.

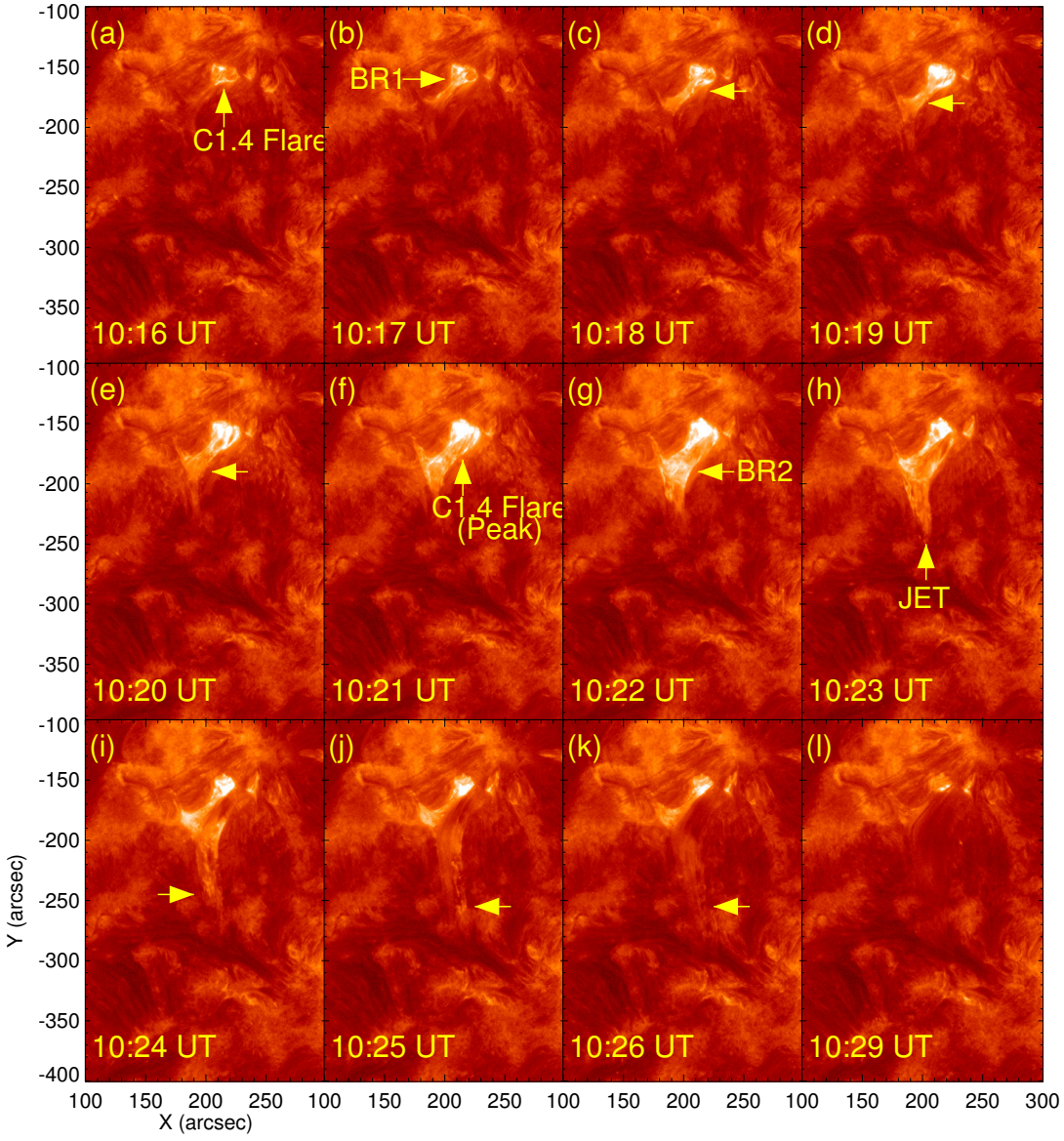

Figure 5.3: Sequence of selected SDO/AIA 304 Å images showing jet eruption.

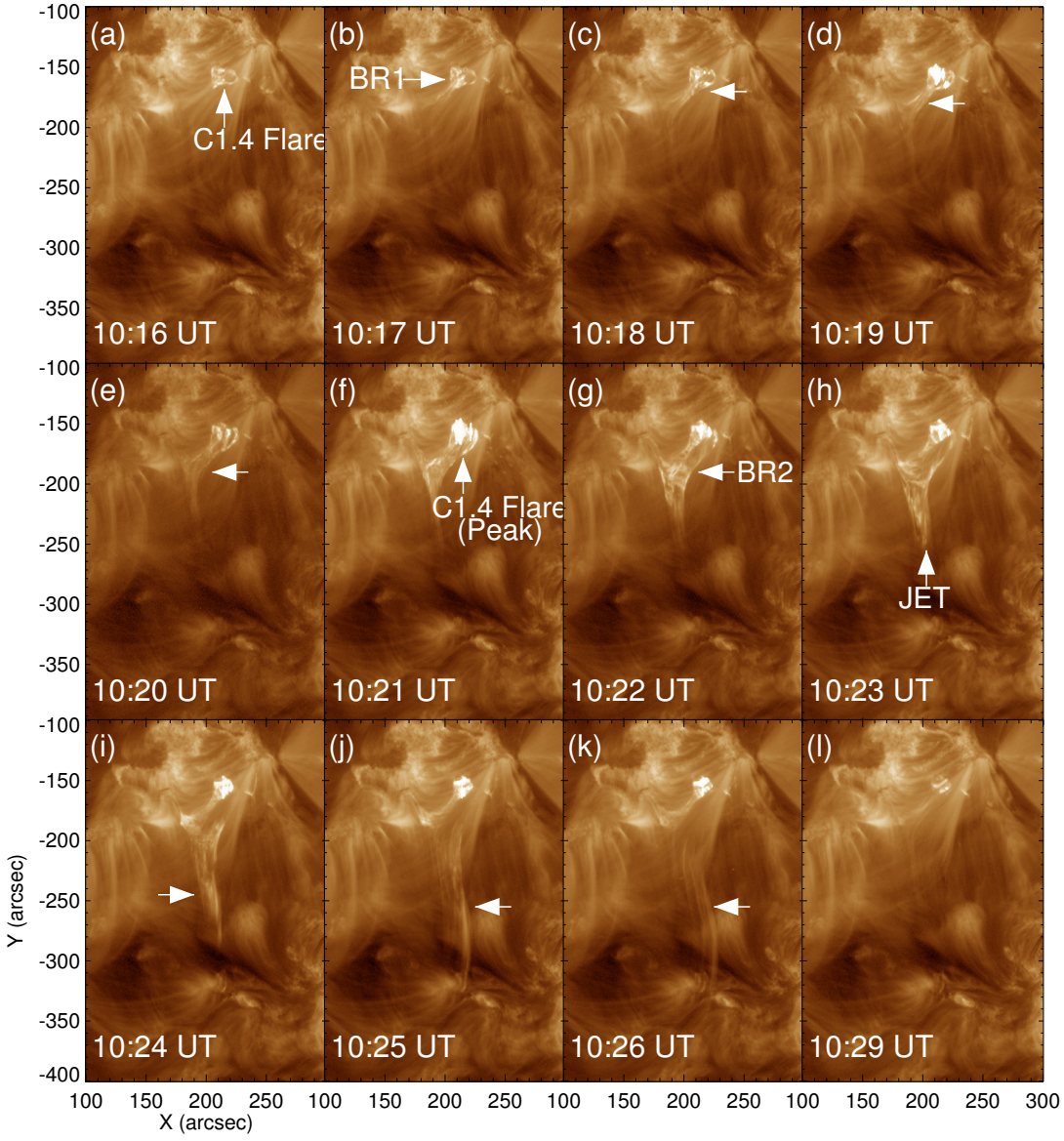

Figure 5.4: Sequence of selected SDO/AIA 193 Å images showing jet eruption.

We describe that the spatial location within black box is associated with a C1.4 class flare, which is also associated with the evolution of a complex coronal jet. We describe the multi-wavelength evolution of this jet in the following subsections.

5.3.2 Jet Behaviour in Different SDO/AIA Filters

The base of the jet and co-spatial C1.4 flare location are visible at the top of the photosphere as visible in the time sequence images of that particular region of interest (ROI) observed in SDO/AIA 1600 Å (cf., Figure 5.2). The selected field of view (FOV) is $100''$ - $300''$ in X-direction and $-400''$ - $-100''$ in Y-direction. In the beginning, there is an intensity enhancement at the edge of the active region AR 12178 in south-east direction of its one big sunspot (Figure 5.2). Brightening is observed at 10:20 UT at the location of [x,y] = [$210''$,$-150''$]. After 3 min., a very faint jet-like spire is visible at 10:23 UT and after 13 min. from the initial time of eruption this whole brightening and jet-like spire disappear at 10:29 UT. This brightening is associated with C1.4 class flare which also triggers first stage of the eruption of coronal jet material (cf., Figure 5.3). Magnetic field intensity extracted from the HMI map, is overplotted on the SDO/AIA 1600 Å image at 10:25 UT, where cyan (gold) shows the positive (negative) polarity (see image j of bottom panel of Figure 5.2). Overlaid HMI magnetogram shows that there is a mixture of positive and negative polarities in this FOV. At the footpoint of the jet, the positive polarity dominates. This is the site where first stage is originated.

The upper chromospheric/TR behaviour of jet evolution is shown in the time sequence images in 304 Å filter (see Figure 5.3). The boundary of active region NOAA AR12178 is very active during the period of 10:00 UT - 11:00 UT, so this contaminates GOES emission close to the time of our jet. C1.4 class flare is erupted at 10:16 UT at the base of the observed jet. At 10:17 UT, first brightening (BR1) is observed near the flaring region and above this region a jet-like spire feature developes. We call this eruption as a first

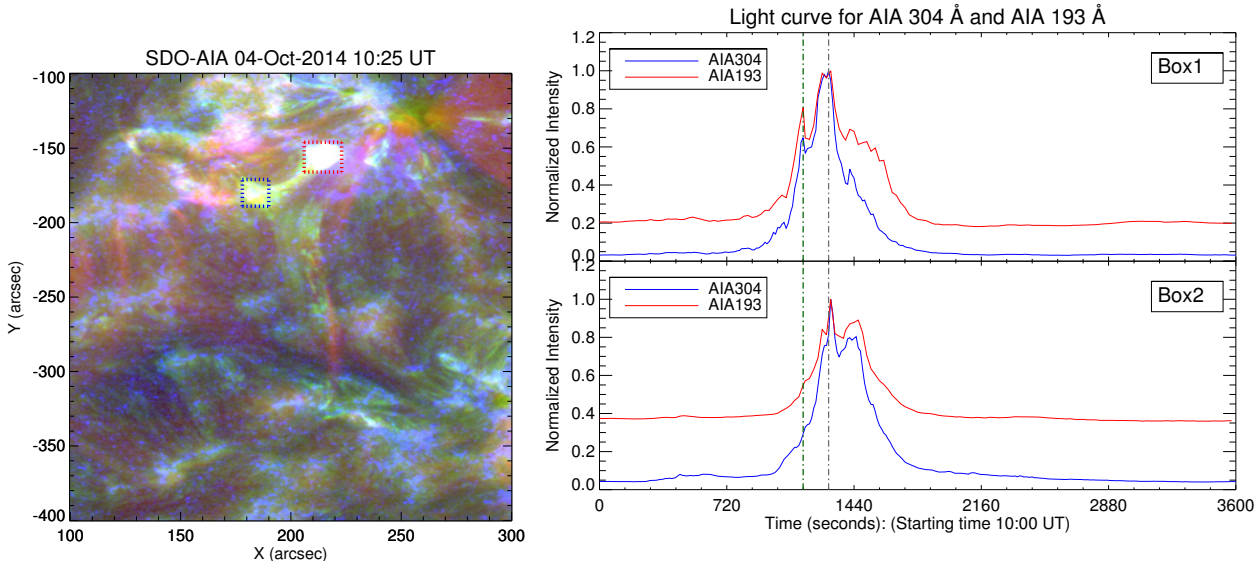

Figure 5.5: Left Panel shows SDO/AIA composite image in 1600 Å, 304 Å and 193 Å depicting the evolution of a confined two-stage coronal jet. Right Panel shows the light curve in AIA304 Å and AIA193 Å , derived from the boxes which are overplotted on the SDO/AIA composite image.

stage of the coronal jet. At 10:21 UT, flare reaches its maximum intensity. At a later time, second brightening (BR2) is observed at 10:22 UT in the overlying corona. Second stage of jet is erupted from this second brightening location upward at 10:23 UT, and reaches its maximum phase at 10:25 UT. The whole feature of jet and brightening go off at 10:29 UT. The behaviour of jet in the coronal region ($\sim 10^6$ K) of the Sun is shown in the temporal sequence images in AIA 193 Å (cf., Figure 5.4). We have selected images at same times as we choose in other SDO/AIA filters to show the jet dynamics at different times at multi-wavelengths.

We have plotted composite image of SDO/AIA at 10:25 UT in AIA 1600 Å , AIA 304 Å , AIA 193 Å to show the jet eruption simultaneously in different temperatures (left panel of Figure 5.5). Two boxes are overplotted on this image, namely, red dotted box and blue dotted box. An intensity lightcurve is plotted in two different AIA filters AIA 304 Å and AIA 193 Å (right panel of Figure 5.5) for the comparison. We have examined the intensity variation for 1-h time period (10:00 UT - 11:00 UT) corresponding

to these two boxes as Box1 (red dotted box; see upper part of right panel of Figure 5.5) and Box2 (blue dotted box; see lower part of right panel of Figure 5.5). The box sizes are taken as $17'' \times 20''$ and $12'' \times 18''$ for Box1 and Box2 respectively. The coordinate of Box1 is $206''$ to $223''$ in X-direction and $-166''$ to $-146''$ in Y-direction and coordinate of Box2 is $178''$ to $190''$ in X-direction and $-189''$ to $-171''$ in Y-direction. We have selected these two boxes, (Box1, Box2) respectively at the footpoint of the jet (origin site of first stage) and the location of second brightening (site of the evolution of second stage). Two dashed lines are overplotted on intensity lightcurve for Box1 and Box2, which represent the 10:19:12 UT, 10:21:36 UT at time axis. We get the peak intensity value at 10:19:12 UT and at 10:21:36 UT for Box1 and Box2 respectively. It can be observed that there is 02:24 min. time delay between the first peaks of intensity for these two boxes. We have noticed in intensity light curve that there is intensity peak shift, as for Box1 as it is observed at 10:19:12 UT, and for Box2 at 10:21:36 UT. There is no time delay in the light curves (193 Å , 304 Å) derived from Box2, (or box1) at different wavelengths. This implies that there is no reconnection at that point and there is only a density (thus intensity) enhancement at that point as the plasma erupted in the first stage of coronal jet arrived at this point. From this point, the jet's plasma is deflected and guided in more southward direction higher into the corona on a curvilinear path which is the effect of the BR2 location. We will describe its theoretical interpretation in Section 5.4.

5.3.3 Evolution of Cool Surge as seen in $H\alpha$ Observations

The behaviour of the cooler component of the jet is shown in the temporal sequence images of GONG $H\alpha$ 6563 Å (cf., Figure 5.6). In $H\alpha$ images, the chromospheric feature of compact flare is clearly visible at 10:16. It initiates and reaches its maximum intensity around, 10:21 UT. Cool surge appear at 10:25 UT after the eruption of the second stage of the coronal jet and attains its maximum height at 10:32 UT. The cool surge exists up

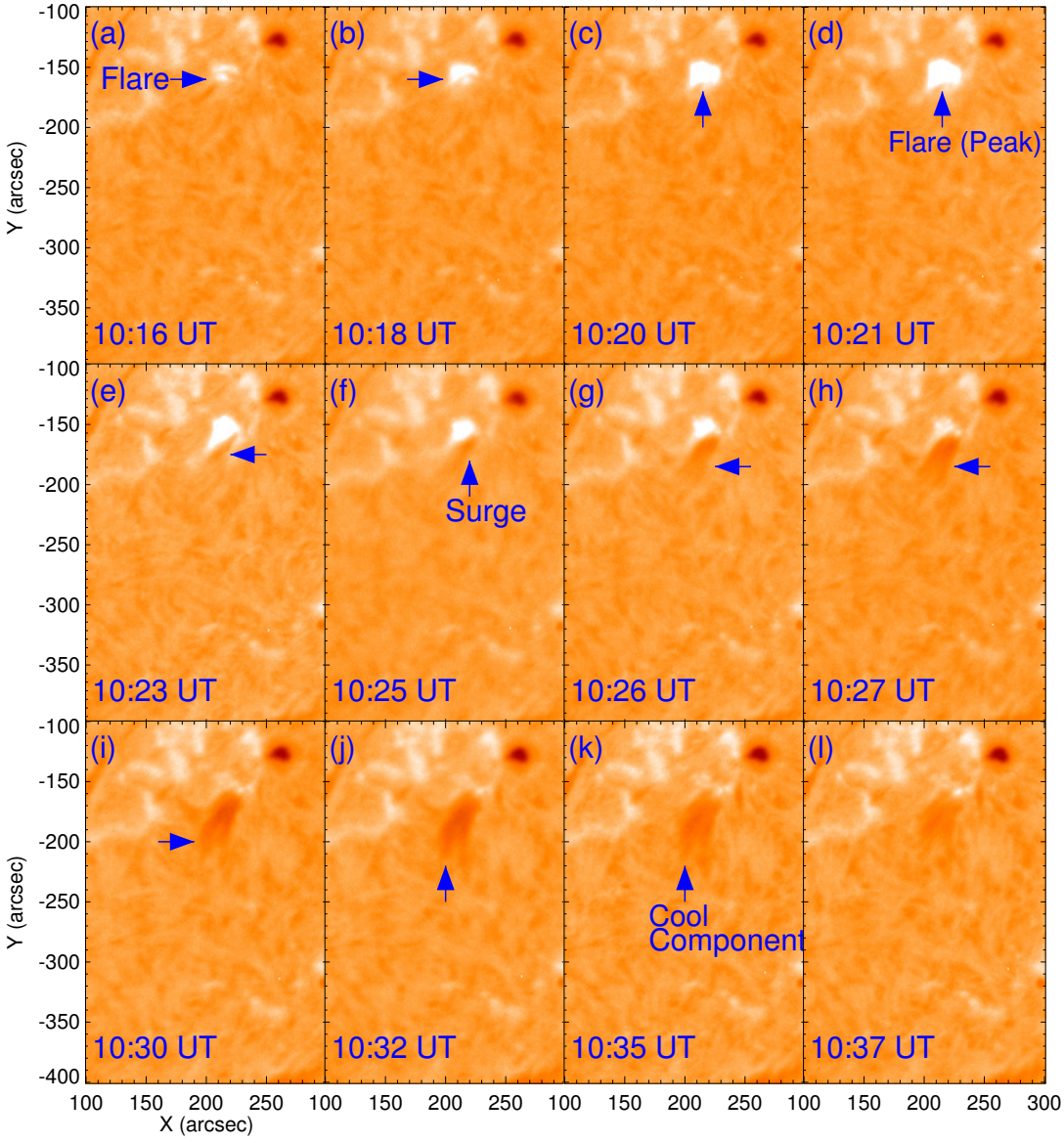

Figure 5.6: Sequence of selected GONG $H\alpha$ 6562 Å images showing cool surge eruption.

to 10:35 UT and completely disappears after 10:37 UT. It should be noted that surge is initiated from the same location as of the coronal jet, and it moves through the same channel where the first stage of jet eruption already moved.

5.3.4 Kinematics of Jet and Associated Solar Surge

The height-time analysis is used to evaluate the kinematics of two-stage coronal jet and associated solar surge. We have done the comparative study of the kinematics of coronal jet and associated surge. Figure 5.7 (bottom panel) shows the height-time diagram for jet (SDO/AIA 304 Å) in bottom-left part and for surge (GONG $H\alpha$) in bottom-right part. The slit position for jet height-time diagram is overplotted on SDO/AIA 304 Å , and slit position for surge height-time diagram is overplotted on GONG $H\alpha$. The slit positions are shown in Figure 5.7 (top panel) where slit position for jet is in top-left panel, and for surge in top-right panel. We choose curved path as the combined path of the two stages of the jet. We have drawn two paths as white-dashed lines on height-time diagram for jet to calculate the speeds of the two stage jet eruption exhibiting a curvilinear motion. For the first stage, jet apparent velocity and acceleration are respectively 91 $\mathrm{km\,s^{-1}}$ and 1 $m\ s^{-2}$. For the second stage jet, apparent velocity and acceleration are 280 $\mathrm{km\,s^{-1}}$ and 10 $m\ s^{-2}$. The height of the first stage is about 20 Mm, and second stage is about 40 Mm. Total time duration of the jet is about 12 min. We have done the height-time analysis for solar surge along the slit position which is shown in Figure 5.7 top-right panel and calculate the apparent velocity and acceleration as 94 $\mathrm{km\,s^{-1}}$ and 4 $m\ s^{-2}$. The height of the solar surge is about 25 Mm.

We have plotted three green-dashed lines on Figure 5.7 where first represents the end time of first stage of the jet, second line represents the start time of the surge and the third one for the end time of second stage of the jet. The cool surge lags behind the coronal

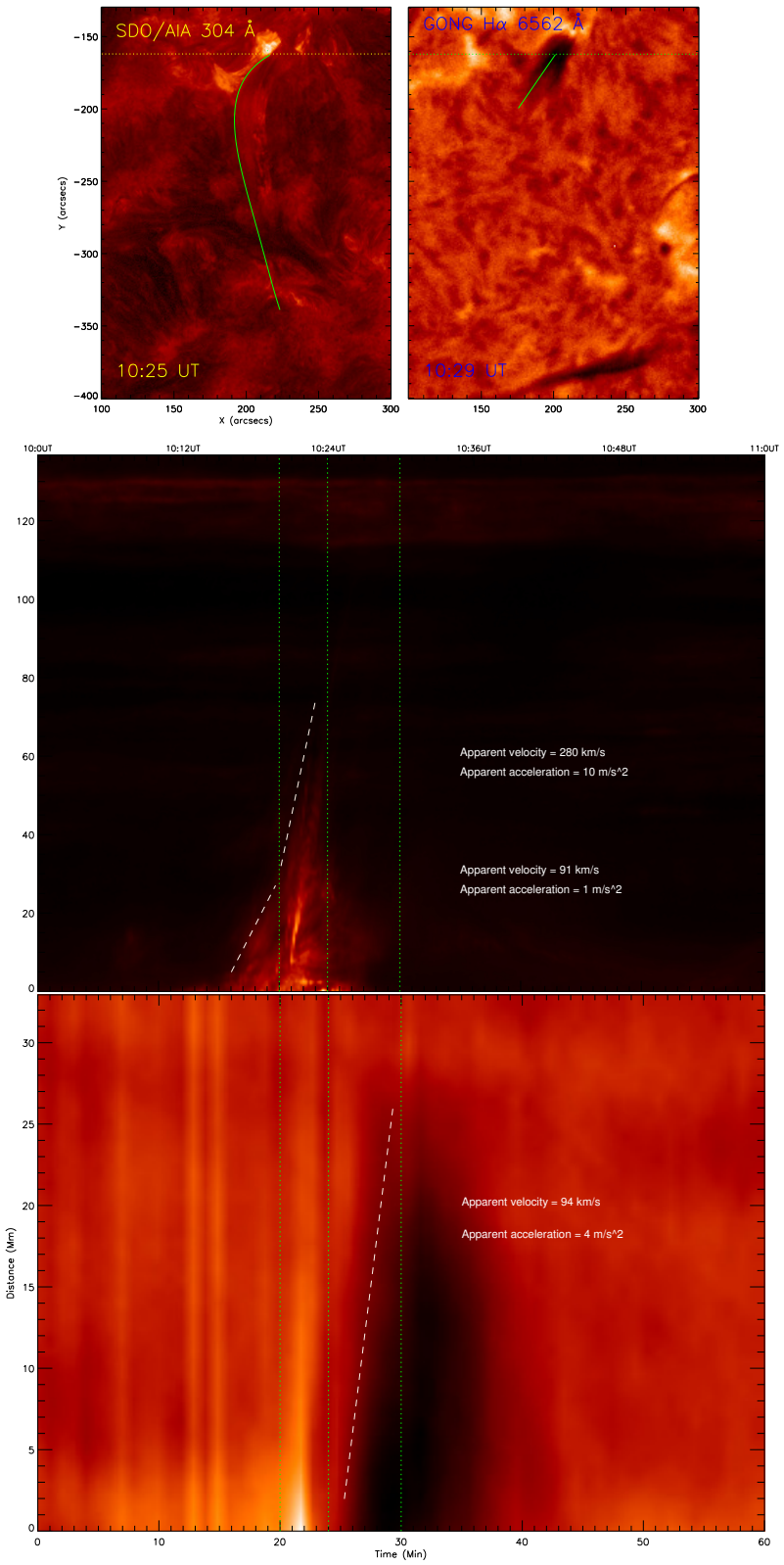

Figure 5.7: Top panel shows the slits position along which Height-Time measurement is done (i) at left side curved slit in AIA 304 Å on 10:25 UT and (ii) at right side vertical slit in GONG $H\alpha$ on 10:29 UT. Bottom panel shows Height-Time Plots (i) in upper part for AIA 304 Å and (ii) in lower part for GONG $H\alpha$.

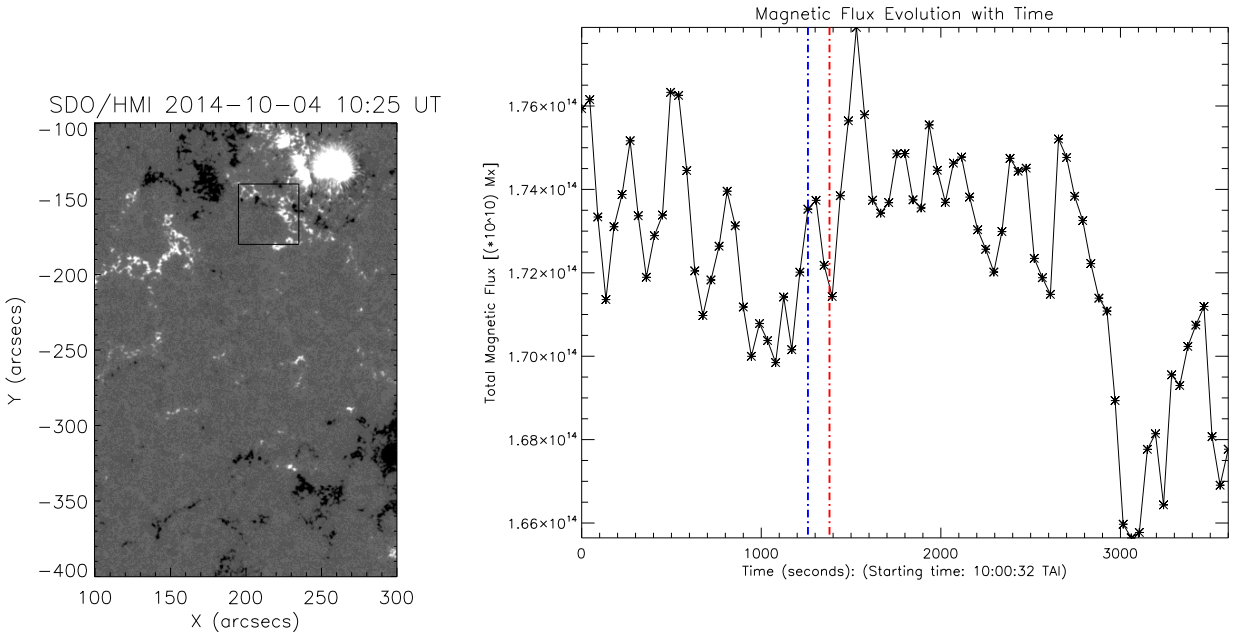

Figure 5.8: Left panel shows SDO/HMI magnetogram at 10:25UT. Right panel shows change in total magnetic flux at the footpoint of the jet with time.

jet. The observed event exhibits the formation of coronal jet that erupts in two stages, and associated cool surge lagging behind it.

5.3.5 Investigation of Magnetic Field Properties at the Base of Jet using SDO/HMI

We study the magnetic field properties at the footpoint of the jet with HMI LOS magnetogram. The origin of jet and compact flare can be inferred using the SDO/HMI data. We derive the total magnetic flux at the base of the jet and triggering site of the compact flare. This flux is derived from a box which is overplotted on the HMI LOS magnetogram at 10:25 UT as shown in the left panel of Figure 5.8. The total magnetic flux is derived from the base of the jet for one hour time duration from 09:59:56 UT to 10:59:56 UT. This variation is shown in right panel of Figure 5.8 where magnetic flux is plotted with respect to time. The total magnetic flux is of the order of 10^{24} Mx.

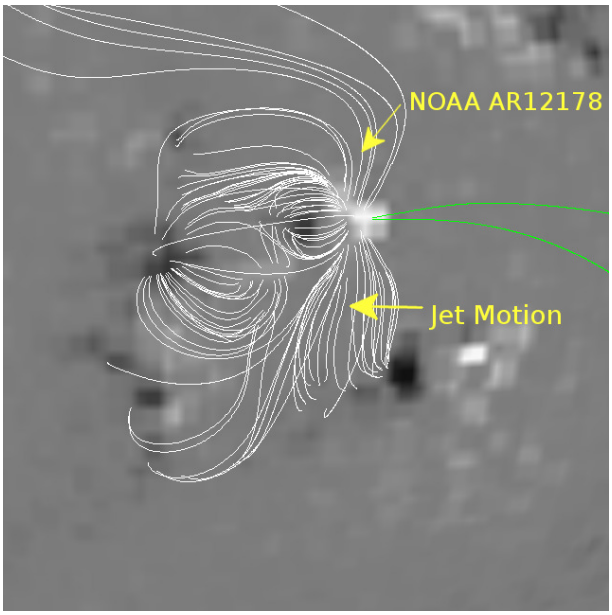

Figure 5.9: Presentation of magnetic field lines around the NOAA AR12178 on 04-Oct-2014 at 12:04:00 UT using the Potential Field Source Surface (PFSS) model. The large-scale magnetic field configuration remains unaltered before and after the evolution of jet between 6:00 UT and 12:00 UT, therefore, we use SOHO/MDI magnetogram that is available just after the jet evolution to understand large-scale field configuration.

Two lines blue and red are overplotted on this figure, where blue line represents 10:21 UT and red line represents 10:23 UT on the time scale. The cancellation rate is $\sim 1.15 \times 10^{23}\ Mx\ h^{-1}$ for the time duration of 10:00 UT to 10:23 UT. It is clear that amount of total un-signed flux decreases upto 10:23 UT. Therefore, the C-class flare and jet eruption both occur. This signify the likely role of the magnetic flux cancellation in the formation of this compact flare and the jet.

5.3.6 PFSS Extrapolation

We analyse the magnetic topology over the active region NOAA AR12178 by using PFSS extrapolation at 12:04:00 UT on 04-Oct-2014. The large-scale magnetic field configuration remains unaltered before and after the evolution of jet between 6:00 UT and 12:00 UT, therefore, we use SOHO/MDI magnetogram that is available just after the jet

evolution to understand large-scale field configuration. Figure 5.9 shows the magnetic field extrapolation generated by PFSS (Schrijver and De Rosa, 2003) code and SOHO/MDI magnetogram. This PFSS package is available in IDL Solar Software (Freeland and Handy, 1998). In Figure 5.9, white and green lines show the closed and open magnetic field lines respectively. Yellow arrow point towards the active region NOAA AR12178.

In Figure 5.9 closed magnetic field lines are shown on the south-east part of the active region which are open up to certain heights in the corona. The two-stage jet is observed along these magnetic field lines in different SDO/AIA EUV filters (304 Å , 193 Å). We observe that the morphology of extrapolated magnetic field lines is similar to EUV images of two-stage jet. Finally, the jet does not go into outer corona and fades away because the magnetic field lines are only open up to certain heights in the corona and they finally connect to a closed path.

5.4 Interpretation

The base of the observed jet is subjected to the magnetic field (positive & negative) cancellation (cf., Figure 5.8) and building up of a C-class flare occurs (Figure 5.1). Thereafter, the jet's first stage erupts and drives the plasma along the field lines (Figures 5.3 - 5.4) until it meets with the discontinuity interface of different set of magnetic field lines lying in its east side and going into the negative magnetic polarities (Figure 5.9).

It should be noted that jet's first stage erupts outwards along the field lines coming out from the big positive polarity sunspot of AR12178 (Figure 5.9). The region where two distinct set of field lines pass near each other can be considered forming some coronal null-points, and these regions show a discontinuity in magnetic field (low) values as well as characteristic plasma speeds (e.g. low Alfvén and fast magnetoacoustic speeds). Therefore, the discontinuity at such X-point pushes and guides further the second stage eruption of the jet's plasma. Therefore, it does not cross, however, towards other side of the distinct

set of the field lines present in the south-east direction of the eruption (Figure 5.9). Second stage of the jet moves more higher into the overlying corona, expands, and shows evolution and kinematics on a curvilinear path (Figures 5.3 - 5.5, 5.7). However, this stage of the jet eruption does not escape as it moves up to some extent above into the corona but within the channel of large-scale closed field lines (Figure 5.9). It gradually fades and disperses in the ambient atmosphere. The evolution of the coronal jet is also associated with the evolution of cool surge (Figure 5.6). Surge is also co-spatial with the C-class flare and jet, however, it lags behind the jet (Figure 5.7). There is no magnetic field cancellation observed at the base (photosphere) associated with the surge on the time of its evolution (Figure 5.8). Therefore, we can infer that the typical flux cancellation scenario and isolated origin of the surge do not work in the present case, and there is an intra-relationship between the evolution of complex coronal jet and cool surge.

It should be noted that the evolution of the first stage of the coronal jet and cool surge are co-spatial and largely confined. The base of the coronal jet shows strong brightening (Figure 5.2), and at later time the base of the cool surge also exhibits brightening (Figure 5.6). Therefore, it is most likely that these two confined ejecta (First stage of the coronal jet and cool surge) are formed by the evolution of the reconnection generated heating pulses at the top of the photosphere (Kayshap, Srivastava and Murawski, 2013; Kayshap *et al.*, 2013; Shibata *et al.*, 1992).

5.5 Discussion and Conclusions

We study the morphological and dynamical characteristics of a two-stage coronal jet which is observed on 04 October 2014 outside the leading Sunspot of NOAA AR12178 using SDO/AIA, GONG $H\alpha$ as well as SDO/HMI magnetograms. The photospheric magnetic field has also been examined at the footpoint of the jet. The main results, of this work are the following:

1. We have done the analysis of photospheric magnetic field at the footpoint of the jet and observe magnetic cancellation which can be a triggering mechanism for the compact flare energy release as well as eruption of the complex two-stage coronal jet.

2. We have done the time-intensity analysis at the base of the jet in different SDO/AIA filters and observe that this jet is associated with EUV brightening at its base. This site is associated with flare energy release and the kinematical motion of jet plasma. The intensity peaks in different AIA filters, which match exactly with the GOES X-ray flux peak. This GOES flare triggers the first stage of the eruption of jet's plasma and the flare's energy accelerates it.

3. The hot component of the jet (EUV jet) has more complex structure because it erupts in two stages. In the first stage, it erupts above the flaring region and the open magnetic field lines in the south-east direction. The presence of another set of field lines (cf., Figures 5.4, 5.9) in the east of this first stage eruption creates a discontinuity of the magnetic field and a kind of localized X-point. This does not allow the jet plasma to go beyond it and the second stage of jet eruption begins on a curvilinear path and moving higher into the corona.

4. The cool component of the jet ($H\alpha$ surge) is smaller than its hot component (EUV jet). The appearance of $H\alpha$ surge and EUV jet is not simultaneous, i.e., it shows the different temporal epoch. The cool component of jet lags behind the hot component of jet. However, they possess intra-relationship rather than individual origin.

5. From the height-time analysis of jet, we calculate the apparent velocity and height for the two stages of jet. For the first stage of the jet apparent velocity and height are 91 $km\ sec^{-1}$ and 20 Mm respectively. For the second stage of the jet, apparent velocity and height are 280 $km\ sec^{-1}$ and 40 Mm respectively.

6. From the height-time analysis of solar surge, we get the apparent velocity and height for surge as 94 $km\ sec^{-1}$ and 25 Mm respectively.

There are several triggering mechanisms proposed for the coronal jets, namely, magnetic reconnection (e.g; Sterling *et al.*, 2015; Yokoyama and Shibata, 1995, 1996), impulsive generation of pressure pulse (Kayshap, Srivastava and Murawski, 2013; Kayshap *et al.*, 2013; Shibata *et al.*, 1982; Srivastava and Murawski, 2011), waves/instability (e.g; Cirtain *et al.*, 2007; He *et al.*, 2009; Nishizuka *et al.*, 2008; Pariat, Antiochos and DeVore, 2009; Zhelyazkov, 2013; Zhelyazkov, Chandra and Srivastava, 2017) and photospheric magnetic field emergence (e.g., Gontikakis, Archontis and Tsinganos, 2009; Guo *et al.*, 2013; Jiang *et al.*, 2007) and flux cancellation (e.g., Chae *et al.*, 1998, 1999; Chen, Jiang and Ma, 2008; Uddin *et al.*, 2012). Many observed jets in the Sun's atmosphere fall in the realm of these theoretical models. Our observed jet exhibits very complex evolution from its origin to its plasma dynamics as well as its intra-relationship with cool surge jet. The present observations possess a rigid constraint on the existing theoretical models based on distinct physical process. In conclusion, our observed jet has a multiple physical effects as explained in the study, and such complex jet motions indicate that more than one physical mechanism are at work in forming such jets in the solar atmosphere. While complex magnetic field structuring also plays a significant role in giving shape to them. Therefore, more appropriate models need to be developed by incorporating the multiple drivers in more complex and realistic magnetic field configuration, as well as realistic solar atmosphere.